Digital Light 3D Printing of Double Thermoplastics with Customizable Mechanical Properties and Versatile Reprocessability

Guangda Zhu, Nadine von Coelln, Yi Hou, Clara Vazquez-Martel, Christoph A. Spiegel, Petra Tegeder, and Eva Blasco**

Dr. Guangda Zhu, Dr. Yi Hou, Clara Vazquez-Martel, Dr. Christoph A. Spiegel, Prof. Dr. Eva Blasco

Institute for Molecular Systems Engineering and Advanced Materials, Universität Heidelberg, Im Neuenheimer Feld 225, 69120 Heidelberg, Germany

Institute of Organic Chemistry, Universität Heidelberg, Im Neuenheimer Feld 270, 69120 Heidelberg, Germany

Email: houyicool@iccas.ac.cn; eva.blasco@oci.uni-heidelberg.de

Nadine von Coelln, Prof. Dr. Petra Tegeder

Physikalisch-Chemisches Institut, Universität Heidelberg, Im Neuenheimer Feld 253, 69120 Heidelberg, Germany

Keywords: additive manufacturing, sustainable polymers, self-healing, material recycling

Abstract: Digital light processing (DLP) is a 3D printing technology offering high resolution and speed. Printable materials are usually based on multifunctional monomers, resulting in the formation of thermosets that cannot be reprocessed or recycled. Some efforts have been made in DLP 3D printing of thermoplastic materials. However, these materials exhibit limited and poor mechanical properties. Here, we present a new strategy for DLP 3D printing of thermoplastics using two polymers with contrasting mechanical properties, where stiff and flexible linear polymers are sequentially constructed. The inks consist of two vinyl monomers, which lead to the stiff linear polymer, and α-lipoic acid to form the flexible linear polymer via thermal ring-opening polymerization in a second step. By varying the ratio of stiff and flexible polymers, the mechanical properties can be tuned with Young's modulus ranging from 1.1 GPa to 0.7 MPa, while the strain at break increased from 4% to 574%. Furthermore, these 3D-printed thermoplastics allow for a variety of reprocessability pathways including self-healing, solvent casting, reprinting, and closed-loop recycling of the flexible polymer, contributing to the development of a sustainable materials economy. Last, we demonstrate the potential of the new material in applications ranging from soft robotics to electronics.

1. Introduction

3D printing is a promising technology for the manufacturing of complex 3D structures.[1–4] In particular, digital light processing (DLP) technology stands out for its high printing resolution and speed.[5–7] During 3D printing, the rapid liquid-solid conversion of printable materials (inks) under light irradiation typically requires the use of bifunctional or multifunctional monomers, resulting in thermosets consisting of permanently covalently crosslinked polymer networks.[8–10] Although the produced thermosets exhibit excellent mechanical properties and chemical resistance, these stable polymer networks also present limitations in terms of adaptivity and reprocessability.[11–14] As a result, the disposal of these 3D-printed thermosets at the end of their service life, may further aggravate the plastic pollution problem that the world is already facing. In contrast, thermoplastics - which consist of non-crosslinked linear polymers - can be reprocessed by melting or dissolving in monomers or solvents,[15–18] making them ideal candidates for a sustainable materials economy. DLP 3D printing of thermoplastics generally requires: 1) rapid photopolymerization of liquid monomers into solid polymers within a few seconds and 2) a high glass transition temperature (T_g) above the print temperature (usually room temperature) or semi-crystallinity of the resultant thermoplastic to effectively hinder the diffusion and dissolution of the formed polymer chain into the surrounding liquid monomers during printing.[17–20] The need for high T_g and semi-crystallinity inevitably results in “just” stiff 3D printed thermoplastics exhibiting Young's moduli usually exceeding 100 MPa, and strains at break below 10%.[17–22] However, emerging fields such as soft robotics and soft electronics, generally require flexible and stretchable materials with Young's moduli of 0.1-10 MPa and high fracture strains >200%.[23–26] Thus, it remains a challenge to DLP 3D print thermoplastics exhibiting flexible and stretchable features, which could meet these application requirements and allow to further expand the application scope.

Double network polymers composed of two different polymers generally exhibit superior properties to those composed of a single polymer.[27–30] For example, by using double network hydrogels consisting of two interpenetrating polymer networks with contrasting mechanical properties, materials that are both hard and strong have been reported, exhibiting features comparable to those of cartilages.[31] The introduction of both stiff and flexible linear polymers in DLP printing would be an elegant approach to overcome the limitations of 3D printed thermoplastics by enabling new and customizable features such as mechanical properties and reprocessability. However, applying this concept - the use of double polymers with disparate mechanical properties – to the DLP of thermoplastics is not trivial. While the printing of stiff linear polymers has been accomplished (see above), the incorporation of flexible linear polymers is challenging. The flexible counterpart can be incorporated either by adding the polymer directly to the formulation or by adding a suitable monomer (small molecule) that enables the formation of the flexible polymer during printing. The first approach leads to an increase in the ink viscosity and high viscosity inks (> 5 Pa.s) are poorly flowable and may not be able to fill the print area before the next layer is produced, thus reducing print efficiency.[32,33] In the second case, the low T_g of the

formed polymer results in a soft thermoplastic that tends to dissolve in the monomer bath, further affecting print resolution and even printability. Thus, DLP 3D printing of flexible linear polymers, and even more the combination of double stiff and flexible systems, has remained a challenge in the field.

Herein, we introduce for the first time a double thermoplastic system consisting of stiff and flexible linear polymers that enables DLP printing of complex 3D geometries with customizable mechanical properties and versatile reprocessability (**Figure 1**). To overcome the aforementioned limitations for 3D printing of thermoplastics, a new strategy is presented (Figure 1a). The stiff and flexible double linear polymers are sequentially constructed from an ink consisting of two vinyl monomers (4-acryloylmorpholine (ACMO) and 1-vinyl-2-pyrrolidone (NVP), blue) that will lead to the stiff linear polymer, and α-lipoic acid (TA, red) as a biobased precursor to form the flexible linear polymer (Figure 1a(i)). First, the stiff linear poly(ACMO-NVP) (P(ACMO-NVP)) polymer with high T_g is formed during the DLP printing process by photopolymerization of the two vinyl monomers in the presence of α-lipoic acid (TA) (Figure 1a(ii)). Subsequently, the ring-opening polymerization of TA forms another linear flexible poly(TA) (PTA) polymer that homogenously blends with the previously formed stiff P(ACMO-NVP) via hydrogen bonding interactions. By varying the ratio of stiff to flexible linear polymers, the DLP-printed 3D thermoplastics exhibit a wide range of mechanical properties, with Young's modulus spanning more than three orders of magnitude (Figure 1b). Furthermore, the non-crosslinking nature of 3D printed thermoplastics allows for a variety of reprocessability pathways (Figure 1c), including i) self-healing, ii) solvent casting, iii) reprinting, and iv) closed-loop recycling of the flexible PTA polymer to the original TA monomer. In addition, the flexible mechanical properties and multiple reprocessability enabled the preparation of self-healing soft actuators and recyclable soft electronics.

2. Results and Discussion

2.1. Ink Design and 3D Printability

In order to sequentially introduce the desired features into 3D printed thermoplastics, we designed an ink formulation for DLP consisting of 4-acryloylmorpholine (ACMO) and 1-vinyl-2-pyrrolidone (NVP) as photosensitive monofunctional monomers and α-lipoic acid (also known as thioctic acid) (TA) (**Figure 2**a). The monofunctional ACMO and NVP were selected as suitable monomers because of their high reactivity and low viscosity. In particular, the monofunctional ACMO can copolymerize with NVP during printing to rapidly form the stiff linear P(ACMO-NVP) (Figure 2b). TA interacts with the formed polymer by hydrogen bonding between the carbonyl group of NVP and the hydroxyl group of TA (Figure 2b). It is important to note that in addition to copolymerizing with ACMO, the NVP monomer also plays an important role as a diluent, ensuring adequate ink viscosity, as the hydrogen bonding between NVP and TA increases the solubility of TA in the formulation. In the subsequent step, a flexible and stretchable linear poly(TA) (PTA) polymer is formed by ring-opening polymerization of the incorporated TA using a post-printing thermal

treatment (Figure 2c). Importantly, the stiff and flexible linear polymers need to be formed in the presented sequential order to ensure good printability.

In order to ultimately achieve the tunable mechanical properties of the 3D-printed double thermoplastics, formulations with different ratios between the vinyl monomers (ACMO and NVP) and the TA were studied. For simplicity, the inks are referred to as 0% TA, 10% TA, 30% TA, and 50% TA, indicating the content of TA. The concentration of the photoinitiator (TPO) was kept constant (1 wt.%) in all the formulations. As shown in **Figure 3**a, the ink without TA (0% TA) is colorless and transparent. The increase in mass fraction of TA resulted in both, the yellow color of the inks and viscosity slightly arising. However, the viscosities were in all cases below 2 Pa·s, making them suitable for DLP 3D printing (Figure 3b).

Another key requirement for DLP printability is the rapid photopolymerization, resulting in the rapid conversion of the liquid ink into a 3D solid polymer. To evaluate the efficiency of the process, droplets of the respective formulations were exposed under UV light irradiation for 10 seconds. After irradiation, the inks formed transparent solid polymer films with transmittance of more than 60% in the visible range (Figure 3c). The photopolymerization kinetics of the inks were monitored by Fourier transform infrared (FTIR) spectroscopy. By tracking the decrease of the absorption peak at ~800 cm^{-1} for the vinyl groups of ACMO and NVP at different times under UV light, the photopolymerization rate of the inks was determined (Figure 3d). As shown in Figure 3e, the conversion in the inks 0% TA, 10% TA, and 30% TA exhibited a sharp increase within the first 10 seconds and reached a plateau at around 80%, indicating rapid and efficient photopolymerization. The slower kinetics of ink with higher TA content (50% TA) may be due to the yellowness of the inks and possible side reactions (e.g., ring-opening polymerization of TA under UV light) that absorb and consume part of the UV radiation energy.[34,35] In addition, the printing parameters of the inks were investigated by evaluating Jacob's working curves. As shown in Figure 3f, the experimental data of curing depth versus different light intensities are in good agreement with the working curve model, indicating that all inks have good curing performance.

To demonstrate the printability of all the inks, we used a 3D hollow icosahedron as a model structure for DLP printing (Figure 3g). As shown in Figure 3h, all inks could be successfully printed into the designed icosahedral structures at room temperature using a commercial DLP 3D printer. The printed structure containing 50 wt.% TA achieved the optimal structural features. Adding a low concentration of Sudan I photoabsorber (0.05 wt.%) to the inks prevents overcuring due to light scattering, thus contributing to improving the printing quality. A variety of complex 3D structures with high structural resolution such as butterfly (Figure 3i), hedgehog (Figure 3j), and lattice (Figure 3k) were successfully fabricated using the ink containing 50% TA and Sudan I. These inks are therefore suitable for the DLP printing of complex structures containing fine features.

2.2. Formation of Double Thermoplastics

As stated above, the incorporated TA can be thermally polymerized by ring-opening polymerization to form flexible PTA[36], and is therefore expected to be introduced as a "flexible counterpart" to modulate the mechanical properties in 3D printed parts. Importantly, this step can be carried out without complex synthetic procedures and stringent reaction conditions, but just by heating the 3D printed structures to 90°C for 10 minutes (**Figure 4**a). To confirm the ring-opening polymerization, ^{1}H-nuclear magnetic resonance (^{1}H-NMR) and X-ray diffraction (XRD) were carried out in the starting material (TA) and PTA (without printing and just heating at 90°C) as reference, and compared with the printed samples before and after thermal treatment at 90°C for 10 min (P(ACMO-NVP)/TA-50% and P(ACMO-NVP)/PTA-50%, respectively). In the ^{1}H-NMR spectra (Figure 4b), the two signals at 3.6 ppm and 3.1 ppm corresponding to the five-membered cyclic disulfide of TA (see Figure S1 for the detailed chemical structure) were employed to monitor the polymerization. After polymerization, the signals decreased and a new signal appeared at 2.8 ppm, indicating that TA was successfully polymerized in both the reference sample (PTA)[36] and the printed sample P(ACMO-NVP)/PTA-50%. In the XRD patterns (Figure 4c), the sharp diffraction peak near $2\theta = 23^{o}$ indicates the presence of TA, due to its high degree of crystallinity, while PTA and P(ACMO-NVP)/PTA-50% show an amorphous structure. The disappearance of the crystalline peak at $2\theta = 23^{o}$ for PTA can further prove the success of the ring-opening polymerization of TA (Figure 4c). The same observation was made for all the other compositions (Figure 4d).

Next, we also characterized the double thermoplastics consisting of P(ACMO-NVP) and PTA polymers in different compositions using FTIR and infrared scattering scanning near-field optical microscopy (IR-SNOM), which is capable of imaging the distributions of chemical species with nanoscale spatial resolution.[37–39] First, the FTIR spectra of the single polymers, PTA and P(ACMO-NVP), were recorded. The characteristic C=O signal appears at ~1707 cm^{-1} for PTA, and at ~1605 cm^{-1} for P(ACMO-NVP) (Figure 4e-f). Subsequently, the obtained FTIR spectra of PTA, P(ACMO-NVP), were compared with the one obtained from the 3D printed double thermoplastics showing the coexistence of both signals at ~1707 $cm^{-1}$and ~1605 cm^{-1}, demonstrating the presence of both polymers (Figure 4g). As expected, the signal at ~1707 cm^{-1} corresponding to the C=O group in the PTA gradually enhanced with the increase of the TA mass fraction employed in the formulation (Figure S2). To get further insides of the distribution of the polymers in the double system, the IR-SNOM spectra of the samples were measured at different positions (Figure 4h-i, Figure S3). All measured positions of the samples P(ACMO-NVP)/PTA-10%, 30%, and 50% exhibited almost identical IR-SNOM spectra with two signals at ~1707 cm^{-1} and ~1605 cm^{-1}, indicating the uniform blending of flexible PTA polymer and stiff P(ACMO-NVP) polymer and the absence of phase separation segregation.

2.3. Mechanical Properties

The mechanical properties of printed objects were investigated in-depth. First,

dynamic mechanical analysis (DMA) was used to determine the T_g and storage modulus of the 3D printed materials using different formulations and at different states. First, the printed linear P(ACMO-NVP) (without TA) showed a high T_g of ~153°C, comparable to that of poly(ACMO) printed from sole ACMO, suggesting that the effect of reactive diluent NVP on T_g is small (Figure S4). With the incorporation of 50 wt.% TA in the formulation, the resulting printed P(ACMO-NVP)/TA-50% also exhibited a high T_g (~141°C) (Figure 5a) prior to thermal treatment. Both samples P(ACMO-NVP) and P(ACMO-NVP)/TA-50% present a high storage modulus of over 2.0 GPa at printing temperature (30°C), showing therefore high stiffness (Figure 5c). After thermal treatment of printed samples containing TA at 90°C for 10 min, the formation of the second flexible linear PTA reduced the T_g of the materials. By adjusting the mass fractions of the TA in the initial formulations (from 0 wt.% to 50 wt.%), T_g could be varied from ~153°C to ~43°C (for P(ACMO-NVP)/TA-50%) (Figure 5a-b) and importantly, the storage modulus at 30°C (printing temperature) was tunable from ~2.0 GPa to ~0.1 GPa (Figure 5c), displaying a wide range of adjustable mechanical properties.

The adjustable mechanical properties can be directly reflected by the degree of deformation of the printed objects under the same stress. As shown in Figure 5d, a hollow icosahedron structure composed of P(ACMO-NVP) polymers could withstand a weight of 1 kg (more than 800 times its weight) without any apparent deformation, indicating high stiffness. In contrast, the icosahedron structure composed of P(ACMO-NVP)/PTA-50% was completely flattened at the same weight, showing its flexibility (Figure 5e). In addition, the P(ACMO-NVP)/PTA-50% sample could be stretched to approximately six times its original length, further showing high stretchability (Figure S5). In order to quantitatively measure the mechanical properties, we performed tensile tests using printed dog-bone-shaped samples (Figure S6). Figure 5f shows the representative stress-strain curves of the printed samples with different mass fractions of flexible PTA. As the mass fraction of flexible PTA increased, the fracture stress decreased while the strain at break increased significantly, indicating that the mechanical properties changed from stiff to flexible. As the mass fraction of flexible PTA increased from 0 wt.% to 50 wt.%, Young's modulus decreased from 1.1 GPa to 0.7 MPa, spanning three orders of magnitude, while the strain at break increased from 4% to 574%, spanning two orders of magnitude (Figure 5g). Compared to previously reported stiff 3D thermoplastics (Young's modulus up to 1.0-2.2 GPa)[17–22], our thermoplastics not only exhibit comparable stiff mechanical properties (Young's modulus up to 1.1 GPa), but more importantly, they fill the gap in flexible mechanical properties that is rarely reported (Young's modulus less than 10 MPa, and strain at break higher than 200%) (Figure 5h, Figure 1b). In particular, Young's modulus of 0.7 MPa and strain at break of 574% for P(ACMO-NVP)/PTA-50% make our printed thermoplastics suitable for soft robotic applications (see Section 2.5) that typically require flexible and stretchable materials with Young's modulus of 0.1-10 MPa and strain at break of >200% (Figure 1b).[23–26]

2.4. Reprocessability of 3D Double Thermoplastics

In addition to the tunable mechanical properties, the double linear polymer system imparts versatile reprocessability. Herein, using P(ACMO-NVP)/PTA-50% as the example, we demonstrated multiple reprocessability pathways for our 3D printed thermoplastics, including self-healing, solution casting, reprinting, and closed-loop recycling of TA (**Figure 6**).

The thermoplastic character allows the printed 3D structures to heal damage quickly through heat-induced interfacial polymer diffusion and entanglement. As shown in Figure 6a, a 3D-printed cat was cut into two separate parts. After heating at 90°C for 10 min, the two parts were quickly healed. No cracks could be observed at the fracture interface after healing (Figure 6b). Furthermore, the mechanical properties of the healed object were also well recovered. In particular, stress-strain curves of the original and healed samples were measured, and no significant changes were observed after healing (Figure S7). Thus, the good healing capabilities of the material can effectively extend their service life (see next section).

In application scenarios where the printed 3D thermoplastic is severely damaged, it can be dissolved in suitable solvents for further processing into a new 2D film. Figure 6c illustrates the possibility of dissolving a damaged sample in a solvent (THF) and further cast into a 2D film. The recycled film exhibited mechanical properties very similar to the original sample (see stress-strain curves in Figure S8).

In addition to recycling into 2D films using solvents, the printed 3D structures can be recycled and reprinted into new 3D structures by taking advantage of their solubility in the monomers. As shown in Figure 6d, the 3D lattice structure was first dissolved in ACMO and NVP monomers. After adding extra TA (to keep the composition of the reprinted 3D structure the same as the original P(ACMO-NVP)/PTA-50%) and the photoinitiator TPO, the regenerated ink could be printed into a new 3D teddy bear structure. The recycled inks had similar Jacob's working curves, and the reprinted objects displayed similar mechanical properties even after two rounds of reprinting (Figure S9), demonstrating excellent reprintability.

Closed-loop recycling through depolymerizing plastics into repolymerizable monomers is considered a solution that retains 100% of the original performance.[40–42] Based on the fact that PTA polymers can be depolymerized to TA due to the reversible disulfide bonding under mild base conditions[36], we investigated the possibility of a closed-loop recycling of TA from our 3D printed structures (Figure 6e-j). Exploiting the different solubility in water, water-insoluble PTA was separated from P(ACMO-NVP) (Figure 6f-h, Figure S10). The obtained PTA was then depolymerized in 0.5 M aqueous NaOH solution (Figure 6i). Finally, the resulting solution was acidified (pH=3–4) with 1 M aqueous hydrochloric acid to protonate and precipitate TA in the form of a yellow powder (Figure 6j) similar to the original TA powder (Figure 6e). FTIR, ^{1}H-NMR, and XRD measurements showed that the chemical and crystal structures of the recycled TA were also maintained, demonstrating its closed-loop nature (Figure S11). The closed-loop recycled TA can be used to prepare new inks for 3D printing, enabling value-added manufacturing and utilization.

2.5. Showcase Applications of 3D Double Thermoplastics

The customizable mechanical properties and versatile reprocessability of our printed dual 3D thermoplastics contribute to their potential in various applications such as soft robotics and soft electronics.

To explore the feasibility of using our 3D thermoplastics in soft robots, we designed and fabricated a healable pneumatic soft actuator (**Figure 7**a-b, Figure S12). The hollow structure of the pneumatic soft actuator was directly fabricated by DLP 3D printing without the need for complex multi-step molding or casting manufacturing processes (Figure 7a). The actuator can be bent when pressure was applied, and returned to its original shape when pressure was released (Figure 7b(i)). Self-healing flexible materials are indispensable for soft robots that need to survive in complex environments where they are susceptible to mechanical damage that can affect their performance.[25,26,43] For example here, once damaged, the actuator lost its deformation ability (Figure 7b(ii)). After healing, the actuator regained its ability to bend similar to the original one when pressure was applied (Figure 7b(iii)), showing that the printed soft actuator using our dual thermoplastic system can be effectively repaired and thus, its service life is extended.

Furthermore, we could upgrade the used or even broken actuator to manufacture soft electronics by taking advantage of its reprintability. Wearable electronics have received great attention from the consumer electronics market and have been growing in recent years.[44–46] It is foreseeable that the widespread application of wearable electronic products will lead to further accumulation of electronic waste in the future. In this scenario, we demonstrate recyclable soft electronics made from our printed thermoplastics (Figure 7c-j). As shown in Figure 7c-f, the used soft actuator was first dissolved in the monomers to obtain a recycled ink, which was then printed into a new grid structure. The structure was coated with a silver paste to enable conductivity. The coated structure was used as a soft wire in a circuit to illuminate an LED (Figure 7g, Figure S13). Wearable electronics could be realized by attaching the conductive soft structure to the fingers or other body parts (Figure 7g). After use, the conductive soft structure was dissolved in monomers to obtain a suspension composed of silver paste and monomer (Figure 7h). After separation, the recycled silver paste could be restored to its original conductivity (Figure 7i, Figure S14), while the obtained monomer solution could be used to fabricate new 3D structures for further applications (Figure 7j). Therefore, all the materials involved were recycled, reducing the environmental impact of discarded soft electronics.

3. Conclusions

In summary, we have presented a new approach for the high-resolution 3D printing of double thermoplastics with highly tunable mechanical properties and versatile reprocessability using two polymers with disparate mechanical properties. The rational design of the inks composed of ACMO, NVP, and TA ensured low ink viscosity (below 2 Pa·s) and fast liquid-solid conversion (below 10 s) for successful DLP

printing. During DLP printing, rapid photopolymerization of monofunctional ACMO and NVP monomers first contributed to a stiff linear P(ACMO-NVP) polymer that ensured printability and high resolution. Subsequently, the incorporated TA enabled the formation of the second flexible linear PTA polymer via ring-opening polymerization. By varying the ratio of stiff and flexible polymers, the 3D printed thermoplastics exhibiting tunable mechanical properties, with Young's modulus ranging from 1.1 GPa to 0.7 MPa, and fracture strain from 4% to 574% were successfully achieved. Furthermore, the non-crosslinked nature of the double linear polymer structures endowed these 3D thermoplastics with a variety of reprocessability pathways, such as self-healing, solvent casting, and reprinting. In addition, the flexible PTA could be separated from the double thermoplastics and depolymerized into TA based on reversible disulfide bonding, enabling closed-loop recycling of TA. Importantly, the successful integration of high-resolution printability with customizable mechanical properties and versatile reprocessability not only expands the range of applications, particularly filling the gap for DLP-printed 3D thermoplastics in soft actuators and soft electronics, but also extends the product lifetime and contributes to the development of a sustainable materials economy.

Acknowledgments

E.B., N.v.C., and P.T. acknowledge the funding from the Deutsche Forschungsgemeinschaft (DFG, German Research Foundation) via the Excellence Cluster "3D Matter Made to Order" (EXC-2082/1-390761711) and the Carl Zeiss Foundation through the "Carl-Zeiss-Foundation-Focus@HEiKA". E.B. and Y.H. also acknowledge the support from the Flagship Initiative "Engineering Molecular Systems" funded by the German Federal Ministry of Education and Research (BMBF) and the Ministry of Science Baden-Württemberg within the framework of the Excellence Strategy of Federal and State Governments of Germany. G.Z. acknowledges the Alexander von Humboldt Foundation for financial support. C.V.M. acknowledges the Fonds der Chemischen Industrie for the support during her PhD studies through the Kekulé Fellowship. The authors thank Florine Sessler for helpful support regarding mechanical testing.

References

[1] R. L. Truby, J. A. Lewis, *Nature* **2016**, *540*, 371.

[2] S. Gantenbein, K. Masania, W. Woigk, J. P. W. Sesseg, T. A. Tervoort, A. R. Studart, *Nature* **2018**, *561*, 226.

[3] B. E. Kelly, I. Bhattacharya, H. Heidari, M. Shusteff, C. M. Spadaccini, H. K. Taylor, *Science* **2019**, *363*, 1075.

[4] H. Le Ferrand, *Acc. Mater. Res.* **2020**, *1*, 123.

[5] D. A. Walker, J. L. Hedrick, C. A. Mirkin, *Science* **2019**, *366*, 360.

[6] M. Dong, Y. Han, X. P. Hao, H. C. Yu, J. Yin, M. Du, Q. Zheng, Z. L. Wu, *Adv. Mater.* **2022**, *34*, 2204333.

[7] X. Kuang, J. Wu, K. Chen, Z. Zhao, Z. Ding, F. Hu, D. Fang, H. J. Qi, *Sci. Adv.* **2019**, *5*, eaav5790.

[8] D. K. Patel, A. H. Sakhaei, M. Layani, B. Zhang, Q. Ge, S. Magdassi, *Adv. Mater.* **2017**, *29*, 1606000.
[9] N. A. Traugutt, D. Mistry, C. Luo, K. Yu, Q. Ge, C. M. Yakacki, *Adv. Mater.* **2020**, *32*, 2000797.
[10] M. Caprioli, I. Roppolo, A. Chiappone, L. Larush, C. F. Pirri, S. Magdassi, *Nat. Commun.* **2021**, *12*, 2462.
[11] B. Zhang, K. Kowsari, A. Serjouei, M. L. Dunn, Q. Ge, *Nat. Commun.* **2018**, *9*, 1831.
[12] G. Zhu, H. A. Houck, C. A. Spiegel, C. Selhuber-Unkel, Y. Hou, E. Blasco, *Adv. Funct. Mater.* **2023**, 2300456.
[13] Y. Jia, H. Xie, J. Qian, Y. Zhang, H. Zheng, F. Wei, Y. Li, Z. Zhao, *Adv. Funct. Mater.* **2023**, 2307279.
[14] G. Zhu, Y. Hou, J. Xiang, J. Xu, N. Zhao, *ACS Appl. Mater. Interfaces* **2021**, *13*, 34954.
[15] T. E. Long, *Science* **2014**, *344*, 706.
[16] C. Jehanno, H. Sardon, *Nature* **2019**, *568*, 2.
[17] S. Deng, J. Wu, M. D. Dickey, Q. Zhao, T. Xie, *Adv. Mater.* **2019**, 7.
[18] G. Zhu, Y. Hou, J. Xu, N. Zhao, *Adv. Funct. Mater.* **2021**, *31*, 2007173.
[19] A. J. Commisso, G. R. Sama, T. F. Scott, *Chem. Mater.* **2023**, *35*, 3825.
[20] M. D. Alim, K. K. Childress, N. J. Baugh, A. M. Martinez, A. Davenport, B. D. Fairbanks, M. K. McBride, B. T. Worrell, J. W. Stansbury, R. R. McLeod, C. N. Bowman, *Mater. Horiz.* **2020**, *7*, 835.
[21] M. Hegde, V. Meenakshisundaram, N. Chartrain, S. Sekhar, D. Tafti, C. B. Williams, T. E. Long, *Adv. Mater.* **2017**, *29*, 1701240.
[22] J. Herzberger, V. Meenakshisundaram, C. B. Williams, T. E. Long, *ACS Macro Lett.* **2018**, *7*, 493.
[23] D. Rus, M. T. Tolley, *Nature* **2015**, *521*, 467.
[24] F. Hartmann, M. Baumgartner, M. Kaltenbrunner, *Adv. Mater.* **2021**, *33*, 2004413.
[25] S. Terryn, J. Brancart, D. Lefeber, G. Van Assche, B. Vanderborght, *Sci. Robot.* **2017**, *2*, eaan4268.
[26] G. Zhu, Y. Hou, N. Xia, X. Wang, C. Zhang, J. Zheng, D. Jin, L. Zhang, *Adv. Funct. Mater.* **2023**, *33*, 2300888.
[27] J. P. Gong, *Science* **2014**, *344*, 161.
[28] T. J. Wallin, L.-E. Simonsen, W. Pan, K. Wang, E. Giannelis, R. F. Shepherd, Y. Mengüç, *Nat. Commun.* **2020**, *11*, 4000.
[29] Z. J. Wang, J. Jiang, Q. Mu, S. Maeda, T. Nakajima, J. P. Gong, *J. Am. Chem. Soc.* **2022**, *144*, 3154.
[30] C. Imaoka, T. Nakajima, T. Indei, M. Iwata, W. Hong, A. Marcellan, J. P. Gong, *Sci. Adv.* **2023**, *9*, eabp8351.
[31] G. Zhang, J. Kim, S. Hassan, Z. Suo, *Proc. Natl. Acad. Sci.* **2022**, *119*, e2203962119.
[32] Z. Weng, X. Huang, S. Peng, L. Zheng, L. Wu, *Nat. Commun.* **2023**, *14*, 4303.
[33] X. Huang, S. Peng, L. Zheng, D. Zhuo, L. Wu, Z. Weng, *Adv. Mater.* **2023**, 2304430.
[34] J. A. Barltrop, P. M. Hayes, M. Calvin, *J. Am. Chem. Soc.* **1954**, *76*, 4348.
[35] G. M. Scheutz, J. L. Rowell, S. T. Ellison, J. B. Garrison, T. E. Angelini, B. S. Sumerlin, *Macromolecules* **2020**, *53*, 4038.
[36] Q. Zhang, Y. Deng, C. Shi, B. L. Feringa, H. Tian, D. Qu, *Matter* **2021**, *4*, 1352.
[37] V. J. Rao, M. Matthiesen, K. P. Goetz, C. Huck, C. Yim, R. Siris, J. Han, S. Hahn, U. H. F. Bunz,

A. Dreuw, G. S. Duesberg, A. Pucci, J. Zaumseil, *J. Phys. Chem. C* **2020**, *124*, 5331.
[38] I. M. Pavlovetc, K. Aleshire, G. V. Hartland, M. Kuno, *Phys. Chem. Chem. Phys.* **2020**, *22*, 4313.
[39] D. E. Halliwell, C. L. M. Morais, K. M. G. Lima, J. Trevisan, M. R. F. Siggel-King, T. Craig, J. Ingham, D. S. Martin, K. A. Heys, M. Kyrgiou, A. Mitra, E. Paraskevaidis, G. Theophilou, P. L. Martin-Hirsch, A. Cricenti, M. Luce, P. Weightman, F. L. Martin, *Sci. Rep.* **2016**, *6*, 29494.
[40] M. Häußler, M. Eck, D. Rothauer, S. Mecking, *Nature* **2021**, *590*, 423.
[41] P. R. Christensen, A. M. Scheuermann, K. E. Loeffler, B. A. Helms, *Nat. Chem.* **2019**, *11*, 442.
[42] Y. Hou, G. Zhu, S. O. Catt, Y. Yin, J. Xu, E. Blasco, N. Zhao, *Adv. Sci.* **2023**, 2304147.
[43] S. Terryn, J. Langenbach, E. Roels, J. Brancart, C. Bakkali-Hassani, Q. A. Poutrel, A. Georgopoulou, T. George Thuruthel, A. Safaei, P. Ferrentino, T. Sebastian, S. Norvez, F. Iida, A. W. Bosman, F. Tournilhac, F. Clemens, G. Van Assche, B. Vanderborght, *Mater. Today* **2021**, *47*, 187.
[44] C. Shi, Z. Zou, Z. Lei, P. Zhu, W. Zhang, J. Xiao, *Sci. Adv.* **2020**, *6*, eabd0202.
[45] M. Baumgartner, F. Hartmann, M. Drack, D. Preninger, D. Wirthl, R. Gerstmayr, L. Lehner, G. Mao, R. Pruckner, S. Demchyshyn, L. Reiter, M. Strobel, T. Stockinger, D. Schiller, S. Kimeswenger, F. Greibich, G. Buchberger, E. Bradt, S. Hild, S. Bauer, M. Kaltenbrunner, *Nat. Mater.* **2020**, *19*, 1102.
[46] B. Shih, D. Shah, J. Li, T. G. Thuruthel, Y. Park, F. Iida, Z. Bao, R. Kramer-Bottiglio, M. T. Tolley, *Sci. Robot.* **2020**, *5*, eaaz9239.
[47] P. H. C. Eilers, *Anal. Chem.* **2003**, *75*, 3631.

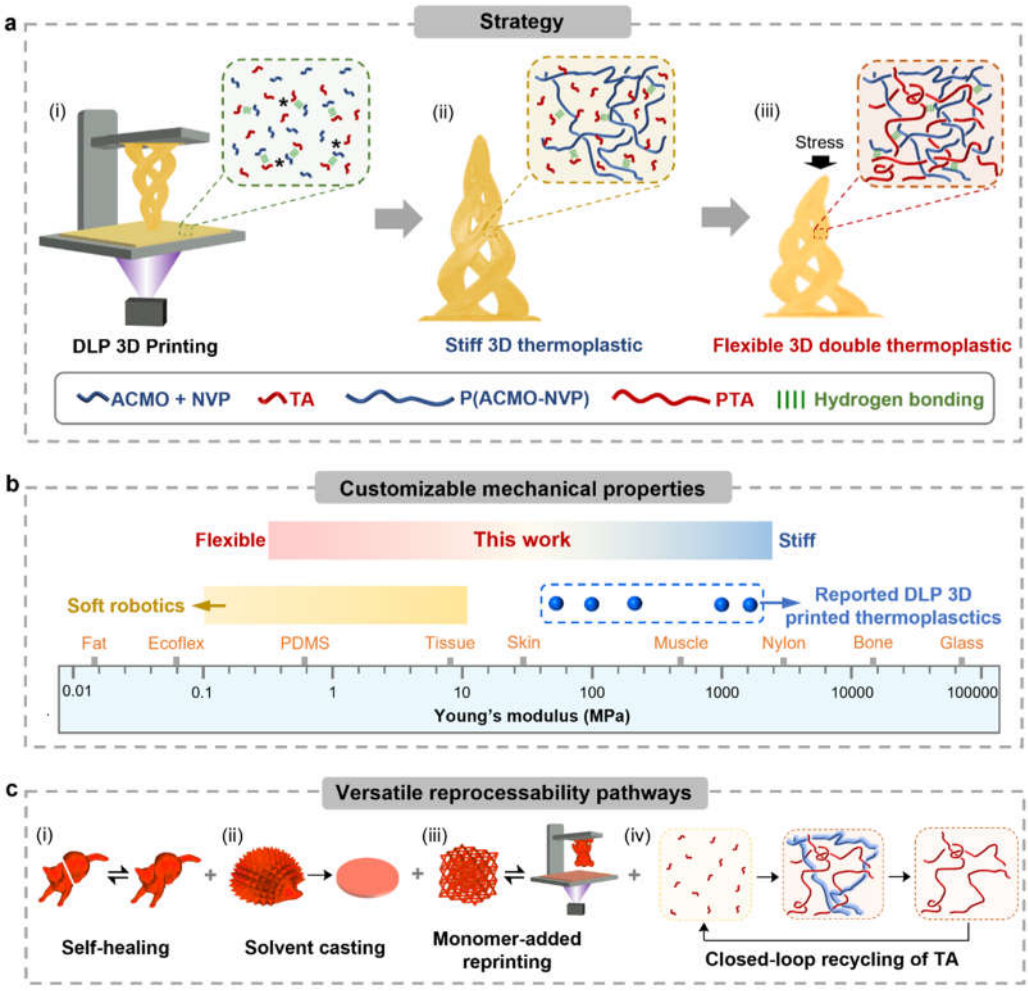

Figure 1. Overview of DLP printed 3D double thermoplastics with customizable mechanical properties and versatile reprocessability. (a) Schematic illustration of the fabrication process of double thermoplastics: (i) DLP printing, (ii) printed stiff 3D thermoplastic composed of a stiff linear polymer, and (iii) flexible 3D thermoplastic composed of stiff and flexible double linear polymers. (b) Customizable mechanical properties ranging from stiff plastics to flexible elastomers. (c) Versatile reprocessability: (i) self-healing, (ii) solvent casting, (iii) monomer-added reprinting, and (iv) closed-loop recycling of TA.

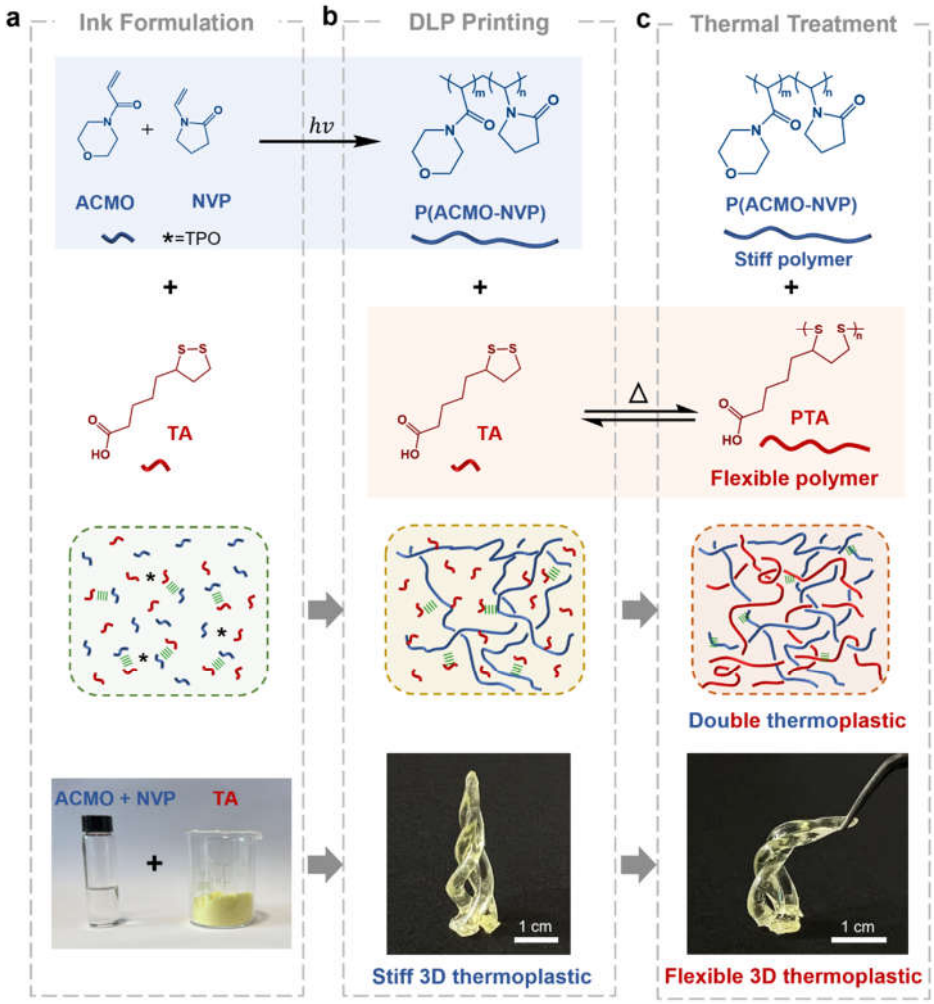

Figure 2. Ink design for DLP 3D printing. (a) Schematic representation of the ink formulation. (b) DLP 3D printing of stiff thermoplastic composed of (ACMO-NVP) in the presence of H-bonded TA. (c) Thermal treatment inducing the ring-opening polymerization of TA and form a flexible double thermoplastic composed of P(ACMO-NVP) and PTA.

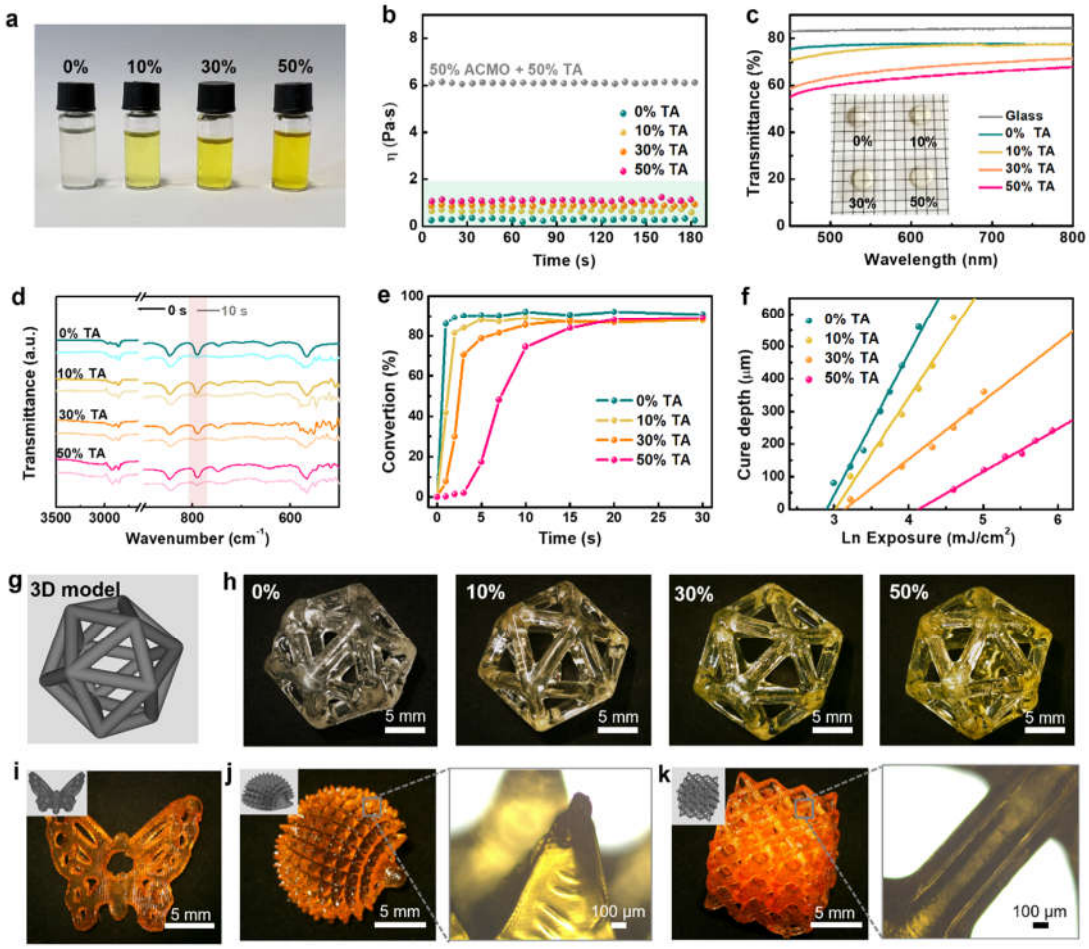

Figure 3. (a) Photograph and (b) viscosity of the inks with different TA mass fractions. (c) UV-visible spectra and photographs of the cured samples (UV curing time: 10 s). (d) FTIR spectra of the inks and UV-cured samples (curing time: 10 s). (e) Reaction kinetics profiles and (f) Jacob's working curves of the inks with different TA mass fractions. (g) 3D hollow icosahedron model for DLP printing. (h) Photographs of printed icosahedron structures using inks with different TA mass fractions. (i-k) Photographs of printed 3D structures using 50% TA ink with 0.05 wt.% Sudan I: (i) butterfly structure, (j) hedgehog structure and its microscope image, (k) lattice structure and its microscope image.

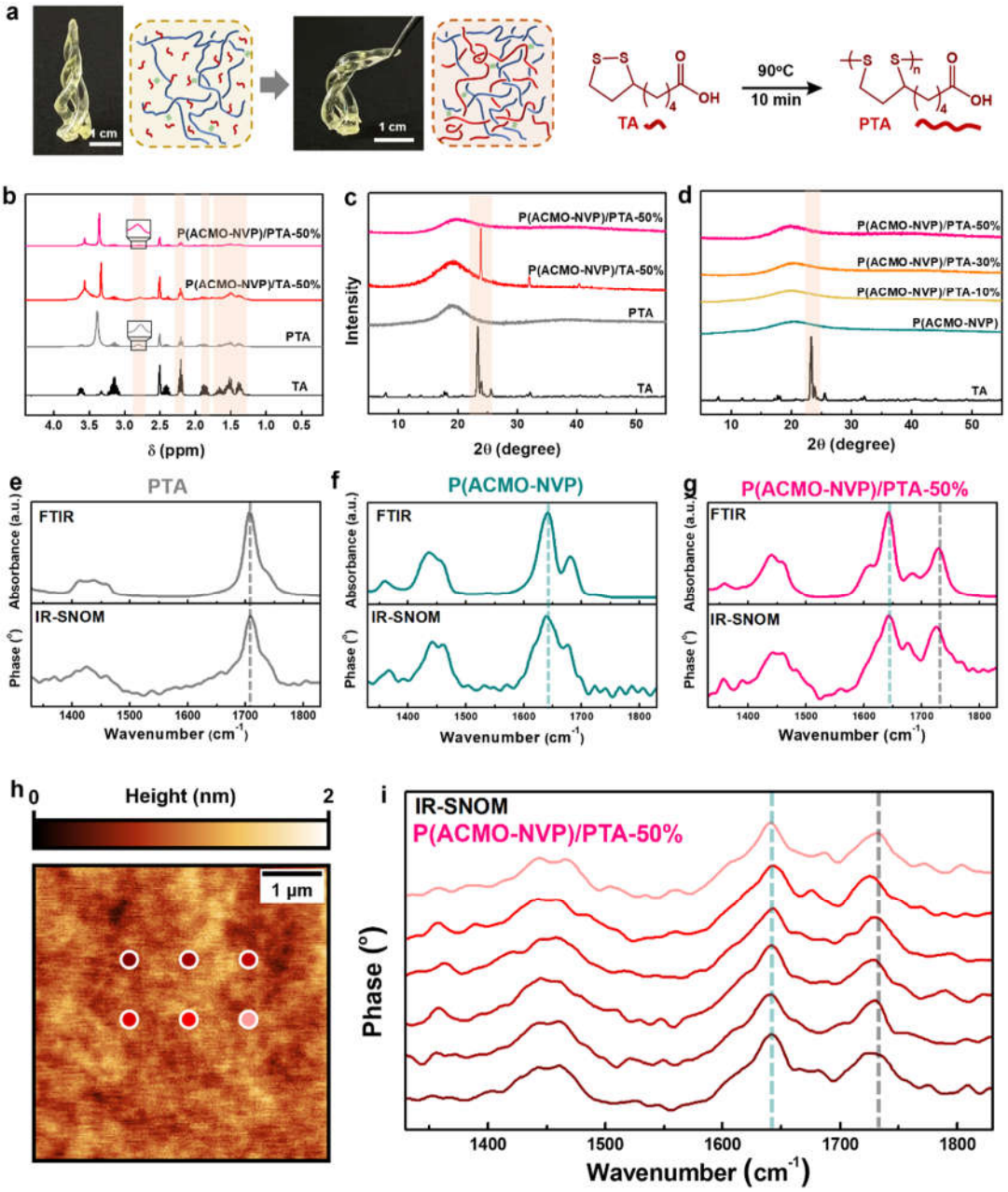

Figure 4. (a) Photographs and schematic representation of the formation of flexible PTA polymer in the printed materials. (b) ^{1}H-NMR spectra and (c) XRD patterns of TA, PTA (references), P(ACMO-NVP)/TA-50%, and P(ACMO-NVP)/PTA-50%. (d) XRD patterns of TA and the samples with different PTA mass fractions. FTIR (top) and IR-SNOM spectra (bottom) of the samples: (e) PTA, (f) P(ACMO-NVP), and (g) P(ACMO-NVP)/PTA-50%. IR-SNOM analysis of (h) the height image of P(ACMO-NVP)/PTA-50% and (i) corresponding IR-SNOM spectra at different positions in (i).

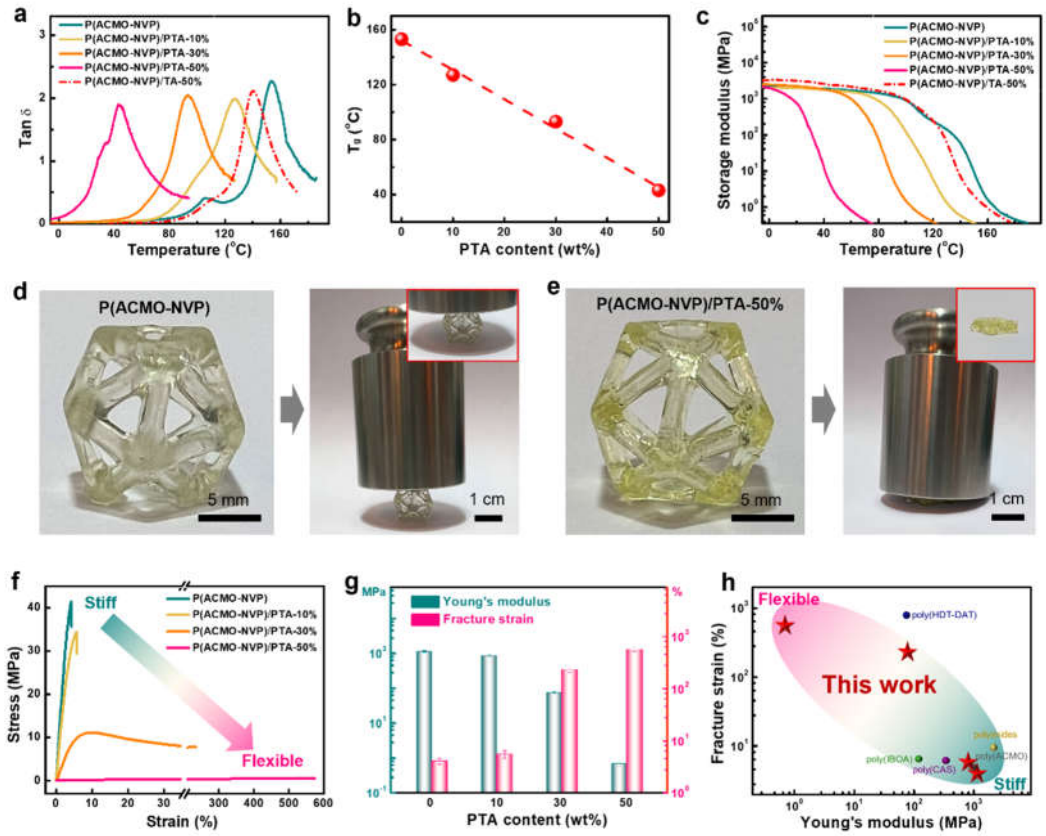

Figure 5. Dynamic mechanical analysis (DMA): the (a-b) T_g and (c) storage modulus of printed objects. (d) Photograph of P(ACMO-NVP) showing its stiffness to withstand the weight. (e) Photograph of P(ACMO-NVP)/PTA-50% showing its flexibility in compression. (f) Stress-strain curves and (g) Young's modulus and fracture strain of printed samples with different PTA content. (h) Comparison of the mechanical properties of this work with reported printed DLP-printed 3D thermoplastics.

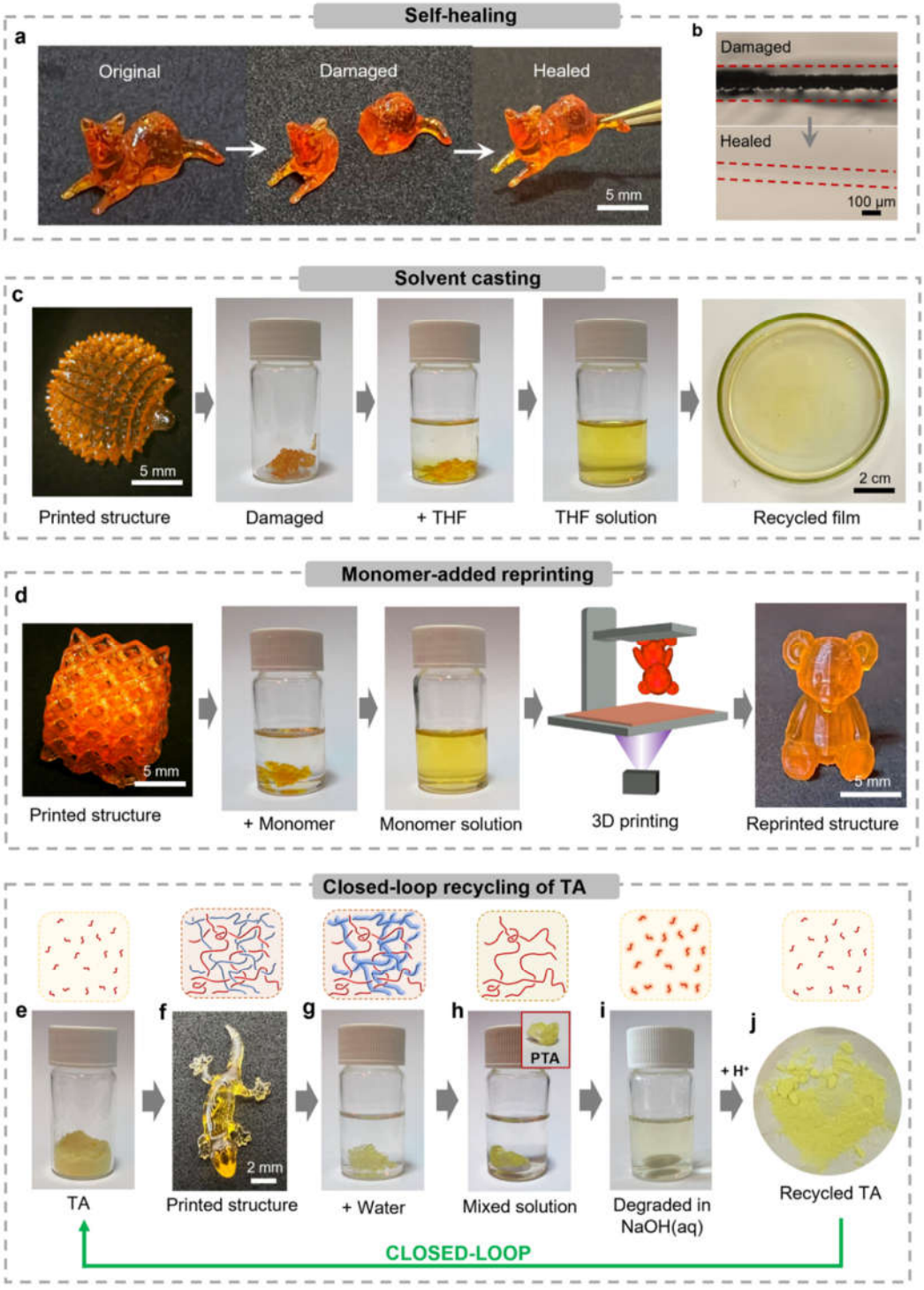

Figure 6. (a) Photographs showing self-healing of the 3D printed cat. (b) Microscopic images showing self-healing of the surface scratch. (c) Photographs showing the solvent casting of a 3D hedgehog structure into a 2D film by using THF. (d) Photographs showing the reprinting of a 3D lattice structure into a 3D bear structure by adding monomers. (e-j) Photographs showing the closed-loop recycling of TA from a printed gecko structure. **Note:** the material employed in all the cases was P(ACMO-NVP)/PTA-50%

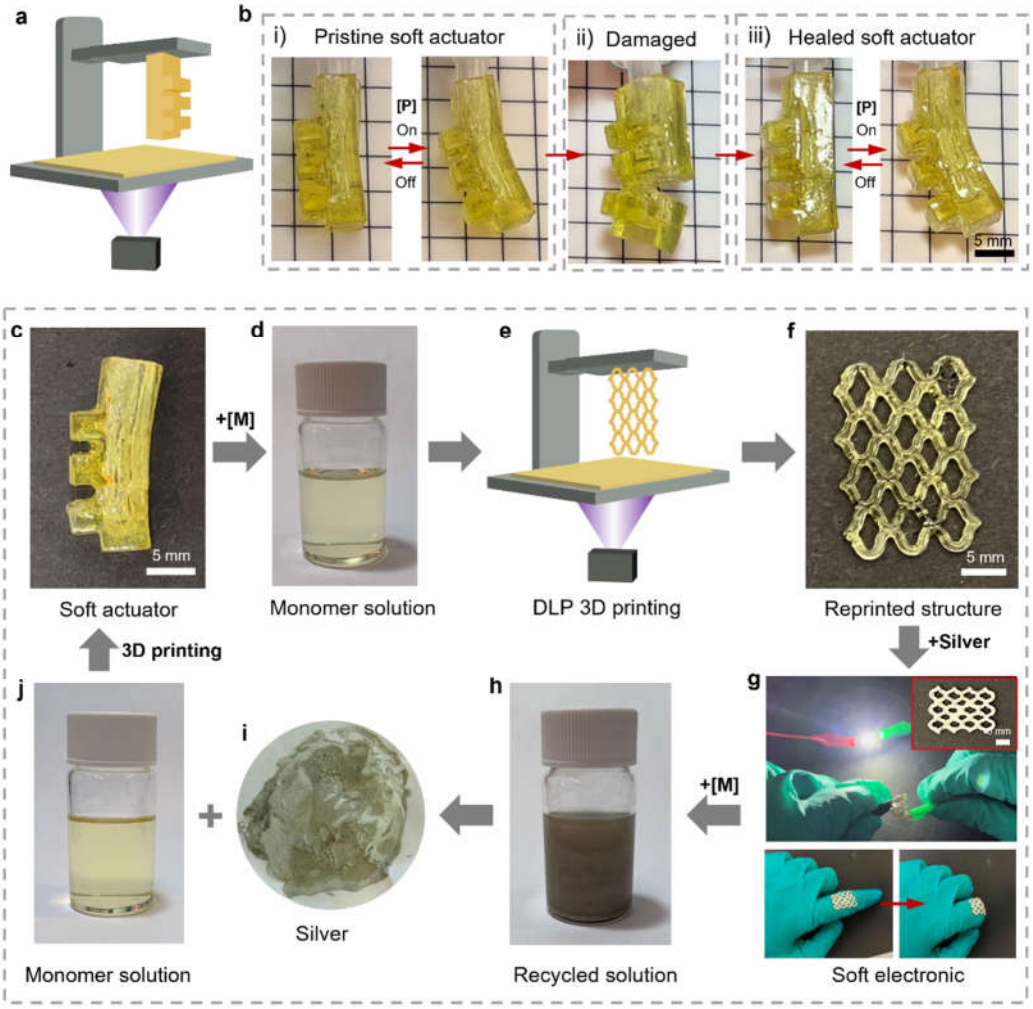

Figure 7. (a) Schematic of DLP printing a soft actuator. (b) Photographs showing the deformation and self-healing of the printed soft actuator. (c-j) Photographs of recyclable soft electronics upgraded from a soft actuator: (c) used soft actuator, (d) monomer solution, (e) DLP 3D printing, (f) the printed grid structure, (g) silver-coated grid structure serving as soft electronics, (h) recycled composite solution, (i) recycled silver and (j) recycled monomer solution. [P] refers to pressure, and [M] refers to monomers of ACMO and NVP.